

UC Irvine

UC Irvine Previously Published Works

Title

Impact of Magnetic Adsorbates on Shallow Nitrogen-Vacancy Centers: Insights from Diamond C(001) Surface Studies

Permalink

<https://escholarship.org/uc/item/1pk475vg>

Journal

The Journal of Physical Chemistry C, 127(37)

ISSN

1932-7447

Authors

Zuo, PJ
Wang, Z
Yu, Clare C
[et al.](#)

Publication Date

2023-09-21

DOI

10.1021/acs.jpcc.3c04026

Copyright Information

This work is made available under the terms of a Creative Commons Attribution License, available at <https://creativecommons.org/licenses/by/4.0/>

Peer reviewed


Impact of Magnetic Adsorbates on Shallow Nitrogen-Vacancy Centers: Insights from Diamond C(001) Surface Studies

P. J. Zuo, Z. Wang, Clare C. Yu, and R. Q. Wu*

 Cite This: <https://doi.org/10.1021/acs.jpcc.3c04026>

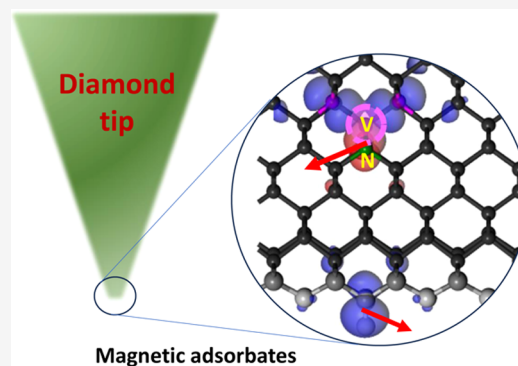
 Read Online

ACCESS |

 Metrics & More

 Article Recommendations

ABSTRACT: Using density functional theory calculations, we investigated the magnetization and magnetic anisotropy of O₂, H, and OH adsorbates on diamond surfaces. Our findings reveal that these adsorbates possess significant magnetic moments, with O₂ having 2.0 μ_B and H and OH having 1.0 μ_B, respectively. Furthermore, they exhibit a non-negligible exchange coupling with the spin of the nitrogen-vacancy (NV) center positioned a few layers beneath the surface. Given the extremely small magnetic anisotropy energies of all of these systems (<1.0 μeV), the presence of magnetic adsorbates is expected to introduce noticeable noise in NV sensing, particularly when NV centers are positioned closer to the surface.



I. INTRODUCTION

The progress in quantum computing and quantum sensing technologies relies on the development of novel materials with tailored properties and a deep understanding of their behavior. Among various approaches, the utilization of electron spins in quantum dots as qubits has been extensively explored, given the robustness of their quantized spin states and the ability to control and measure their evolution using electromagnetic stimuli. Developing materials that can offer robust and isolated quantum spin units, high tunability, and swift control is a formidable challenge. To this end, the nitrogen-vacancy (NV) center in diamond has attracted significant attention as a versatile spin qubit, quantum sensor, and optical emitter.^{1–3} The remarkable properties of the NV center arise from its spin 1 electronic configuration in its negatively charged state (denoted as NV⁻ below, in contrast to the neutral NV⁰). The energy splittings between $S_z = 0, \pm 1$ in its ³A₂ and ³E₂ triplet states of NV⁻ are sensitive to the presence of magnetic and electric fields, as well as lattice strain and temperature changes. These characteristics, along with the NV center's atomistic nature within a solid host environment make it an ideal sensor for various applications, including high-resolution scanning probe microscopy,^{4–8} biomarker detection in living organisms,⁹ and stationary probes in diamond sensor chips.¹⁰ Additionally, NV centers have been explored as sensitive magnetometers, electrometers, pressure sensors, and thermometers.^{11–14}

Quantum sensing with NV centers has been a topic of extensive research over the past decade. The integration of NV centers into scanning probe microscopy has enabled magnetic

field imaging with sub-100 nm resolution for various nanoscale structures, including magnetic structures, vortices, domain walls, superconducting vortices, and electric current mapping.^{14–18} To further enhance the sensitivity and spatial resolution of these probes, it is anticipated that the NV center should be moved closer to the surface of diamond.^{15,16} Nonetheless, it has been noted that the physical properties and quantum states of NV centers can be influenced by adsorbates and defects located on or near the surface.¹⁷ When NV centers are positioned closer to the surface, their coherence times experience a rapid decline, starting at a depth of 22 nm, which is attributed to fluctuations in the surface spin bath.¹⁸ Roskopf et al. discovered that the spin relaxation times of shallow NV centers can be shortened by up to 30 times due to strong thermal fluctuations caused by paramagnetic impurities with small magnetic anisotropy energies. Their research also revealed a high density of surface impurities, estimated to be within the range of 0.01–0.1 μ_B/nm², which may have contributed to the observed reduction in spin relaxation times in the ultrashallow region (<5 nm beneath the surface).¹⁰ Chrostoski et al. employed the Langevin method to simulate the magnetic noise and explore the effects of paramagnetic impurities on H-, O-, and F-terminated diamond surfaces

Received: June 14, 2023

Revised: August 16, 2023

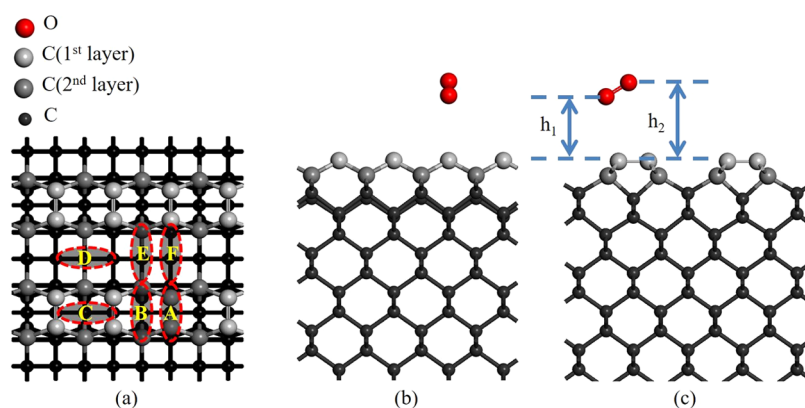


Figure 1. (a) Top and (b, c) side views of different adsorption geometries of O_2 (red spheres) on the C(001) slab. The light gray and dark gray spheres represent the 1st- and 2nd-layer carbon atoms, while the black spheres represent the interior carbon atoms. A–F and red ellipses denote the sites and orientations of the atoms of O_2 ; h_1 and h_2 represent the heights of two oxygen atoms from the surface plane.

within a thin layer of water.¹⁹ Their investigation primarily centered on the noise spectrum associated with spin precession and spin flip phenomena without specifically identifying the sources of impurities.

In the presence of a magnetic adsorbate, the model spin Hamiltonian of the system can be described as

$$H = g_{\text{NV}}\mu_{\text{B}}\mathbf{S}_{\text{NV}}\cdot\mathbf{B} + A_{\text{NV}}S_{\text{NV},z}^2 + J(z)\mathbf{S}_{\text{ad}}\cdot\mathbf{S}_{\text{NV}} + A_{\text{ad}}S_{\text{ad},z}^2 + g_{\text{ad}}\mu_{\text{B}}\mathbf{S}_{\text{ad}}\cdot\mathbf{B} \quad (1)$$

Here, μ_{B} (0.0578 meV/T) is the Bohr magneton; \mathbf{S}_{NV} and \mathbf{S}_{ad} are the spins of the NV and adsorbate, respectively; g_{NV} and g_{ad} are their corresponding g -factors; and A_{NV} and A_{ad} are their magnetic anisotropy energies. For NV^- , A_{NV} determines the zero-field splitting between the $m_s = 0$ and $m_s = \pm 1$ triplet state (2.87 GHz). Obviously, $\langle J(z)\mathbf{S}_{\text{ad}} \rangle$ represents the energy produced by the effective magnetic field acting on the NV spin due to the adsorbate. To avoid significant perturbation of the magnetic resonance measurement, this term should be smaller than a few nano-electrovolts (at the level of MHz). $J(z)$ includes the exchange and magnetic dipole–dipole interactions between the magnetic adsorbates and the spin of the NV center (for simplicity, we only use the z -component of their separation, where the z -axis is perpendicular to the surface). For the contribution of a single magnetic dipole, we may estimate that $J(z) = \frac{53.6}{z^3}\mu\text{eV}/\text{\AA}^3$ and hence z , the distance of the NV center below the surface, needs to be at least 30 Å to satisfy this criterion. As a result, the presence of magnetic adsorbates is detrimental to the NV probe, even when the exchange interaction is neglected.

To address the magnetic noise from surface adsorbates affecting the NV probe, several key questions need to be investigated. (1) Identifying adsorbates with nonzero S_{ad} : Understanding which adsorbates possess nonzero spin values is crucial for determining their potential impact on NV centers. Various surface species, including transition metal ions, organic radicals, or paramagnetic defects, could contribute to magnetic noise. To this end, it is natural to begin by focusing on adsorbates that are abundant in the environment such as O_2 and water vapor derivatives such as H and OH. (2) Understanding the function $J(z)$ and the anisotropy energy A_{ad} : This knowledge can aid in developing strategies to minimize magnetic noise for ultraslow NV centers. (3) Eliminating magnetic adsorbates that plague NV probes:

Developing effective methods to remove or mitigate the influence of magnetic adsorbates on NV centers is vital.

Systematic density functional theory (DFT) calculations offer an effective approach to address these questions regarding the impact of adsorbates on the NV centers in diamond. Accounting for potential adsorbates from air, free O_2 molecules exhibit a spin triplet configuration with a magnetic moment of $2.0\mu_{\text{B}}$ and are paramagnetic in the liquid phase. Prior research has shown that O_2 can form a two-dimensional Kondo magnetic lattice on Au(110) and produce magnetic noise on superconductors with aluminum oxide surfaces.^{20–22} Additionally, both theoretical and experimental evidence suggest H atoms as another potential source of magnetic noise on aluminum oxide surfaces.^{23,24} On diamond surfaces, an isolated H atom can introduce an unpaired electron, resulting in local spin polarization. It is crucial to first investigate the effects of these adsorbates on pure diamond surfaces using DFT studies, which can reveal specific surface configurations and adsorption sites that either promote or suppress magnetization and magnetic coupling. Achieving a comprehensive understanding of the various adsorbates' influence on NV centers in diamond and devising strategies to mitigate their effects are essential for advancing the use of NV centers in quantum sensing, quantum computing, and other quantum technologies.

In this study, we utilize density functional theory to investigate the most probable magnetic adsorbates from air, specifically, O_2 and water vapor derivatives (H atom and OH), on the (001) surface of diamond with a neutral NV^0 center at different depths below the surface. We find that these adsorbates retain their large magnetic moments on C(001) and exhibit extremely small magnetic anisotropy energies. The exchange coupling between their spin moments and the NV spin is weak, yet not negligible, even when the NV center is situated 8–9 layers beneath the surface. Due to the exceedingly small magnetic anisotropy energies of these adsorbates ($<1\mu\text{eV}$), their spin fluctuations are expected to generate substantial noise that alters the quantum energy levels and reduces the coherence times of the NV center. Considering the relatively weak chemical interaction between the adsorbates and the NV center when they are more than 1 nm apart, we believe that the main conclusions regarding adsorption sites, adsorption energy, and magnetic states of adsorbates remain unchanged on a diamond surface with a negatively charged NV^- center. Thus, our findings highlight the need to consider

several potential magnetic sources that can adversely affect NV probes.

II. METHODS AND MODEL

Although it is desirable to directly calculate systems with adsorbates on carbon surfaces featuring NV⁻ centers and diverse surface orientations, the computational requirements for such calculations continue to pose a challenge. This includes addressing the technical difficulties associated with adsorbates and charged surface models. DFT calculations for charged periodic systems with adsorbates are especially problematic due to the necessity for proper charge compensation and the persistent issue of poor convergence behavior, even with attempts such as a recent one described in refs 25,26. Furthermore, simulating NV centers situated a few nanometers deep necessitates the use of large surface models, which also present formidable challenges for the current computational resources. In this study, our focus is on the potential magnetization of adsorbates and their coupling to the spin of the NV center. To model the C(001) surface, we employed a slab consisting of 18 carbon layers and introduced NV centers at varying depths to investigate the *z*-dependence of *J*(*z*). Moreover, to make our DFT calculations more manageable, we opted for NV⁰ (*S* = 1/2) centers instead of NV⁻ centers.

As depicted in Figure 1, we used a 4 × 4 supercell in the lateral plane, containing more than 300 atoms, to simulate the sparse adsorption of O₂, H, and OH on the dimerized diamond surface. A vacuum region of ~15 Å was added to separate the repeating slabs along the *z* axis. The lattice constant in the lateral plane was fixed according to the optimized dimensions of bulk diamond (*a* = *b* = *c* = 3.573 Å), which is consistent with the most recent experimental data, 3.567 Å.²⁷ DFT calculations were performed using the Vienna *ab initio* simulation package (VASP).^{28,29} The exchange–correlation interaction among valence electrons was described by the spin-polarized generalized-gradient approximation with the Perdew–Burke–Ernzerhof functional (GGA-PBE).³⁰ The van der Waals correction was incorporated by using the DFT-D3 method. The interaction between valence electrons and ionic cores was treated within the framework of the projector augmented wave (PAW) method.^{31,32} We set the energy cutoff for the plane-wave bases to 500 eV and utilized a 5 × 5 × 1 *k*-mesh³³ to sample the essentially two-dimensional Brillouin Zone. The positions of adsorbates and carbon atoms in the top 12 layers were fully relaxed using a criterion that the force acting on each atom became smaller than 0.01 eV/Å. The bottom 6 layers of carbon atoms and the passivating hydrogen atoms remained fixed at their bulk-like positions. Based on the authors' experience and prevailing literature, the selected approach and parameters are proven to be effective for examining adsorption systems. While more sophisticated functionals such as hybrid and GW might offer enhanced band gaps and heightened reliability, executing such calculations remains impractical for the surface systems discussed here.

For the determination of magnetic anisotropy energy (MAE), spin–orbit coupling (SOC) is incorporated into calculations with 10 × 10 × 1 *k* points for surface systems. In this work, MAE is obtained by integrating the torque, which is the angular derivative of the spin–orbit coupling Hamiltonian with respect to the polar angle θ of the spin moment away from the O–O bond, i.e.,

$$\tau(\theta) = \frac{\partial E_{\text{total}}(\theta)}{\partial \theta} = \sum_{\text{occ}} \psi_{i,k} \left| \frac{\partial H_{\text{SO}}}{\partial \theta} \right| \psi_{i,k} \quad (2)$$

Integrating τ from 0 to θ gives the angle dependence of the total energy, represented as $E(\theta)$. The torque approach has been effectively employed in studies of various magnetic materials, including the magnetic noise of O₂ on the Al₂O₃(0001) surface.^{21,34,35}

III. RESULTS AND DISCUSSION

For clarity, we will discuss each system's results individually before delving into broader discussions.

1. Adsorption of Oxygen Molecules on a Pristine Diamond Surface—O₂/C(001). The C(001) surface features a (2 × 1) reconstruction with rows of symmetric carbon dimers that saturate the dangling bonds resulting from cleavage. Our calculated dimer length (1.382 Å) is shorter than the carbon bond length in bulk diamond (1.543 Å), which is consistent with experimental data^{36–39} and previous theoretical findings.^{40,41} The first question we seek to answer is whether O₂ can stably adsorb on a clean diamond surface while maintaining its triplet state. To this end, we examined six different adsorption configurations for O₂ on the C(001) surface, as illustrated in Figure 1a. The binding energy per adsorbate is defined according to

$$E_b = E_M + E_{\text{C}(001)} - E_{\text{M/C}(001)} \quad (3)$$

Here, $E_{\text{M/C}(001)}$ is the total energy of M/C(001) (*M* represents adsorbates including O₂, H, or OH), $E_{\text{C}(001)}$ is the total energy of the pristine C(001) surface, and E_M is the total energy of the isolate adsorbate. According to the binding energy (E_b) values listed in Table 1 for various adsorption sites, configuration D

Table 1. Binding Energies (Per Oxygen Molecule) and the Heights of the Two Oxygen Atoms for the Different O₂/C(001) Adsorption Geometries Shown in Figure 1a

adsorption sites	E_b (eV)	<i>h</i> (Å)
A.	0.078	$h_1 = 3.01, h_2 = 3.66$
B.	0.077	$h_1 = 3.08, h_2 = 3.53$
C.	0.068	$h_1 = h_2 = 3.38$
D.	0.144	$h_1 = h_2 = 2.41$
E.	0.128	$h_1 = h_2 = 2.61$
F.	0.134	$h_1 = h_2 = 2.37$

represents the most stable adsorption geometry for the oxygen molecule. In this configuration, O₂ lies in the trench between two parallel rows of carbon dimers, with the O–O bond aligned perpendicularly to the C=C dimers. In this configuration, both oxygen atoms are at the same height, 2.41 Å above the plane of carbon dimers. The magnitude of E_b , approximately 0.144 eV per molecule, indicates that O₂/C(001) involves weak physisorption. This energy is similar to the adsorption energy of O₂ on Al₂O₃(0001), indicating that O₂ molecules may desorb from the surface at temperatures exceeding 50 K.²² However, due to the abundance of O₂ in the environment and the complexity of diamond surfaces, we still anticipate that the presence of O₂ molecules on the surface of NV probes is quite likely. Experimental observations show no oxygen adsorption when the diamond (110) surface was exposed to O₂, but reconstructed diamond (111) and (110) surfaces may adsorb O₂ even at room temperature.^{42,43}

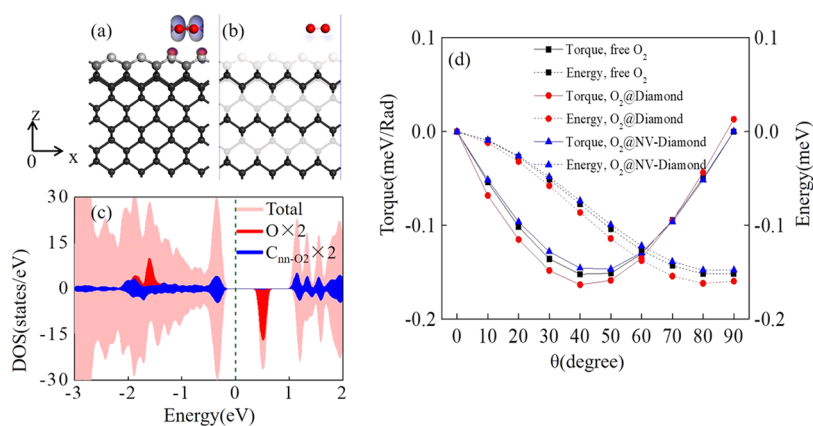


Figure 2. (a) Side view of the optimized structure of $O_2/C(001)$, together with the isosurfaces of the spin density at $\pm 0.001 e/\text{\AA}^3$ (red balls are oxygen atoms; blue and red isosurfaces are for positive and negative spin densities, respectively). (b) Charge density difference in the plane containing two O atoms (blue and red colors represent charge accumulation and depletion, respectively). (c) Projected-DOS of O_2 molecule (red) and its carbon neighbors (C_{nn-O} , blue) (both magnified by a factor of 2), accompanied by the total DOS of $O_2/C(001)$ (peach). The positive and negative values correspond to states in the majority and minority spin channels, respectively. (d) Calculated torques (solid lines) and relative total energies (dashed lines) versus the spin orientation with respect to the O–O bond for the free (black) and adsorbed O_2 molecule (red on pristine C(001) and blue on NV-defected C(001)).

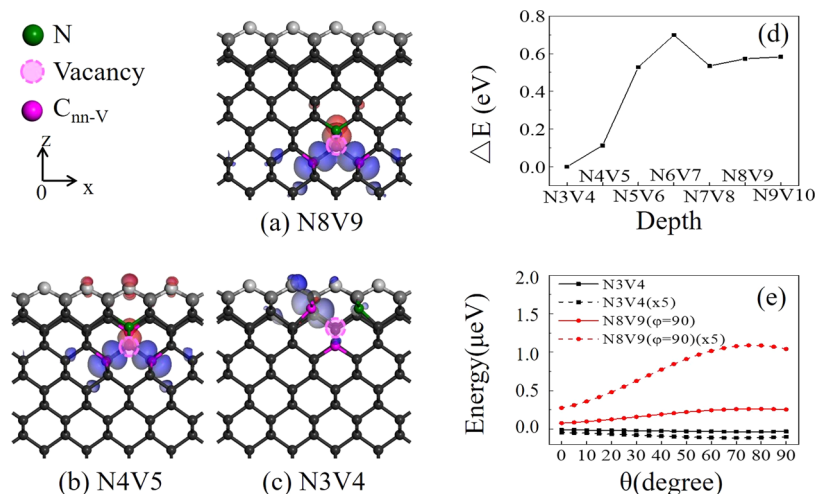


Figure 3. (a–c) Side views for optimized structures of C(001) with NV at different locations. The nitrogen atom and vacancy are represented by a green sphere and a pink translucent sphere, respectively. The magenta spheres highlight the carbon atoms closest to the vacancy. The blue and red isosurfaces ($\pm 0.001 e/\text{\AA}^3$) represent the positive and negative spin densities, respectively. (d) Relative energies (ΔE) for structures with different NV locations. (e) Calculated energies versus the spin orientation away from the z-axis with natural (solid lines) and magnified (dashed lines, by a factor of 5) SOC strengths. The energy curves are shifted vertically for clarity.

Due to the weak interaction with the diamond surface, the adsorbed oxygen molecule maintains a significant spin moment and magnetizes the adjacent C atoms. The total magnetic moment for the system remains close to $2.0 \mu_B$ per O_2 molecule with the spin polarization of O_2 extending to the neighboring carbon atoms. The spin density of the adsorbed O_2 molecule, as shown in Figure 2a, exhibits the donut feature of its $pp\pi^*$ orbital, which is like that of a free O_2 molecule. The charge density redistribution for $O_2/C(001)$, as shown in Figure 2b, reveals that the charge rearrangement is minimal, further indicating a weak interaction between the O_2 and C(001) surface. In line with this observation, Bader charge analysis indicates a minuscule charge transfer of $0.02e$ from the nearest carbon atoms to the O_2 molecule. The total density of states for the $O_2/C(001)$ [represented by the gray background in Figure 2c] and the projected density of states (PDOS) of the O_2 molecule [depicted by the red peaks in Figure 2c]

demonstrate that the $pp\pi^*$ orbitals of the O_2 molecule in the minority spin channel are not affected much by the charge rearrangement associated with adsorption.

We further calculated the magnetic anisotropy energy of $O_2/C(001)$, i.e., the energy barrier for spin rotation, through the torque method.⁴⁴ From the curves of $\tau(\theta)$ and $E(\theta)$, we can observe that the lowest energy corresponds to the case where the spin aligns perpendicular to the O–O bond ($\theta = 90^\circ$), and the energy difference between $\theta = 0$ and 90° is 0.163 meV per O_2 . This value is very close to that of the free O_2 molecule, which is 0.152 meV . As previously mentioned, the magnetic anisotropy of O_2 originates from the SOC interaction between its $pp\pi^*$ orbitals in the two spin channels.²¹ Since the energy barrier for spin rotation around the O–O bond is extremely small for the $O_2/C(001)$, [$\sim 1 \mu\text{eV}$ or 10 mK], which is almost below the limit of precision that DFT can achieve, this rotation is essentially unrestricted. Consequently, spin fluctuations of

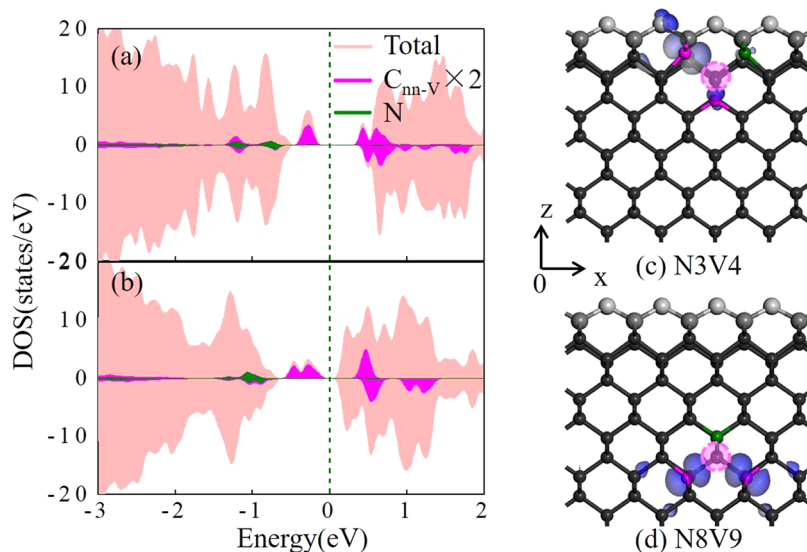


Figure 4. (a, b) Projected-DOS of C_{nn-v} (magenta, magnified by a factor of 2) and nitrogen atom (green), along with the total DOS of NV center diamond surface (peach) for (a) N3V4 and (b) N8V9. The positive and negative values correspond to states in the majority and minority spin channels, respectively. (c, d) Wave function distributions of states within an energy window from -0.5 to 0.0 eV (with isosurfaces at 0.001 e/Å³). The nitrogen atom and vacancy are represented by the green sphere and pink translucent spheres, respectively. The magenta spheres highlight the carbon atoms nearest to the vacancy.

the O₂ can potentially serve as a source of magnetic noise on the C(001) surface at low temperatures.

2. NV Center at Different Depths below the Diamond Surface. In this study, the focus lies on investigating the magnetization of adsorbates such as O₂ and their interaction with the spin moment of an NV center beneath the surface. An intriguing aspect to explore is the distance at which the magnetic adsorbate and NV center need to be separated before $J(z)$ decays to a negligible level. Understanding this decay behavior could provide valuable insights into optimizing the performance of diamond-based magnetometers and sensing devices that utilize NV centers. Given that the exchange coupling is primarily mediated by conduction electrons in the diamond lattice, the results obtained for the neutral NV⁰ state, especially the strength of $J(z)$, are anticipated to be qualitatively applicable to the NV⁻ state. Additionally, the neutral NV⁰ state (spin 1/2) has also been suggested as a sensitive magnetometer for specific applications.⁴⁵

The magnetic properties of the neutral NV center were initially investigated at various depths beneath the surface. To simplify the discussion, NiV_j is used to represent the location of the NV center, with nitrogen at the i^{th} layer and a vacancy at the j^{th} layer below the surface. Interestingly, the total magnetic moment for the NV⁰ center remains consistent at $1.0 \mu_B$ across all cases, demonstrating its stable 1/2 spin 1/2 nature. However, the distribution of spin polarization varies drastically, especially as the NV center moves closer to the surface. In Figure 3a, we observe the spin density for the case where nitrogen is positioned at the eighth layer and the vacancy at the ninth layer (N8V9). The three carbon atoms closest to the vacancy (C_{nn-v} , denoted in purple) exhibit the highest contribution to magnetization, with their dangling bonds oriented toward the vacancy. In contrast, the two carbon atoms in the tenth layer display spin densities opposite to the carbon atom in the eighth layer. This behavior differs from that of the NV⁻ center, where the three neighboring carbon atoms surrounding the vacancy contribute equally to local magnetization in the triplet ground state.

Quantitatively, the C local magnetic moments associated with the N8V9 geometry are $0.347 \mu_B$ for the two C atoms in the 10th layer and $-0.228 \mu_B$ for the C atom in the eighth layer. The N atom also contributes a small magnetic moment of $0.016 \mu_B$. This pattern persists in the N5V6 geometry as seen in Figure 3b, but the local magnetic moments change to 0.381 , 0.272 , and $-0.179 \mu_B$ for the three carbon atoms due to the further reduction in local symmetry. In the case of N3V4, more pronounced changes occur. As shown in Figure 3c, the spin density is primarily concentrated around the C atoms in the third layer, which possess a local magnetic moment of $0.392 \mu_B$. Conversely, the local magnetic moments of the two C atoms in the fifth layer diminish to $0.014 \mu_B$ and $0.018 \mu_B$. Since the total magnetic moment remains at $1.0 \mu_B$ for all of these cases, the magnetization in the interstitial region is also significant.

As shown by the relative energies in Figure 3d, shallow NV centers have a tendency to migrate toward the surface. The energy decreases by 0.6 eV as we move from the N9V10 configuration (the deepest) to the N3V4 configuration (the shallowest) in our model. This can be attributed to the surface region's enhanced capability to accommodate local relaxation and dangling bonds associated with the vacancy. The PDOS curves for both N3V4 and N8V9 display notable gap states in Figure 4a,b, respectively. Due to the reduced symmetry and the Jahn–Teller effect, the e_{xy} orbitals in the majority spin channel experience an energy split. For the N3V4 case, the e_y orbitals around the carbon atoms in the third layer have lower energy, and the e_x orbital in the fifth layer is about 0.9 eV higher in energy compared to undisturbed C atoms. In the N8V9 configuration, the energy splitting between e_x and e_y orbitals is about 0.3 eV. To substantiate these claims, the wave functions of the occupied gap states are displayed in Figure 4c,d.

As expected from the weak SOC of both C and N, the MAE of a single NV is extremely small, even when the SOC strength is artificially increased by a factor of 5 in calculations. The calculated angle-dependent energies of the NV⁰ center at two locations are shown in Figure 3d. For the N3V4 configuration,

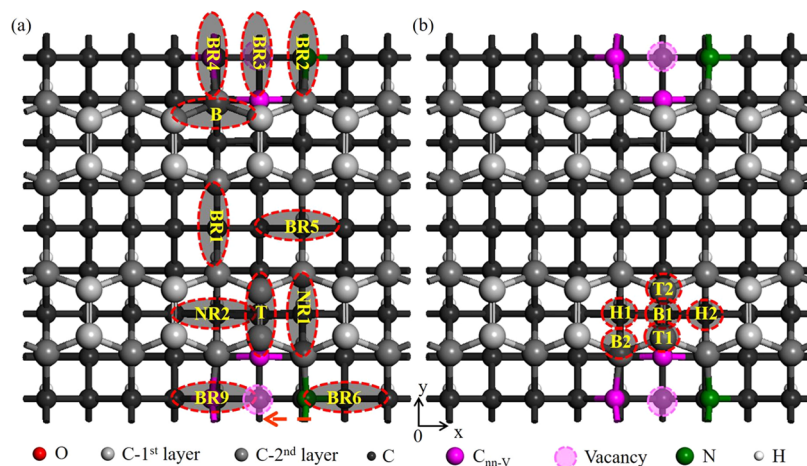


Figure 5. Top view for different adsorption geometries of (a) O_2 and (b) H and OH adsorption sites on the C(001)-N3V4 surface. The color code for the carbon spheres is the same as that in Figure 1. The pink translucent spheres and magenta spheres represent vacancies and their nearest neighbor carbon atoms, respectively.

the MAE is essentially zero according to the torque calculation, as the angular dependence of the energy is negligible ($<0.1 \mu\text{eV}$), even with the enhanced SOC. In the case of N8V9, the energy change remains less than $0.1 \mu\text{eV}$ (or $0.8 \mu\text{eV}$ with the amplified SOC), with a slight preference for the spin to align along the z -axis (the axis connecting N and V). However, these MAEs are already too small for conventional DFT calculations, even with the use of the torque approach. Note that the MAE for an $S = 1/2$ system will not affect its two quantum levels. For NV^- , an $S = 1$ system, the MAE due to SOC is also exceedingly small, $<0.1 \mu\text{eV}$. Therefore, the zero-field splittings of the triplet states should not be attributed to SOC but rather the dipolar interaction between the spins on the 3 carbon atoms nearest to the vacancy, as discussed by Gali.¹²

3. O_2 Adsorption on C(001) in the Vicinity of an NV Center. The presence of the NV center reduces the symmetry of the C(001) surface, resulting in more nonequivalent adsorption sites for the adsorbates, as illustrated in Figure 5a. To quantify the strength of the O_2 adsorption, we calculate the binding energy using eq 3, where $E_{\text{C}(001)}$ is replaced by the total energy of the C(001) substrate containing an NV center. Based on the binding energies of O_2 at different adsorption sites, the most stable adsorption geometry occurs when O_2 occupies the BR9 site on C(001)-N3V4, similar to its position on pristine C(001). In this configuration, the oxygen molecule is situated in the trench between two rows of carbon dimers, with the O–O bond oriented perpendicular to the C–C bonds and one O atom positioned above the carbon vacancy, as depicted in Figure 5a.

Interestingly, this geometry retains the lowest energy as the NV center moves further into the interior region, indicating that the surface chemistry is not significantly influenced by the NV center when it is more than 3 layers beneath the surface. Nonetheless, subtle changes in the heights (h_1 and h_2) are observed, as shown in Table 2. Notably, the O_2 molecule exhibits a slight tilt on the C(001)-N3V4 surface due to the stronger attraction between the vacancy site and the adsorbed O_2 compared to the nitrogen atom.

As depicted in Figure 6a–c, the cation of O_2 receives a small amount of charge from the substrate across all three structures. Consequently, the binding energies of O_2 in the presence of an NV center are slightly higher than those on pristine C(001). In

Table 2. Binding Energies (Per Oxygen Molecule) and Heights of Oxygen Atoms Measured from the Topmost C Layer of the $\text{O}_2/\text{C}(001)\text{-N3V4}$ in Different Geometries, as Depicted in Figure 5

adsorption sites	E_b (eV)	h (Å)
T	0.070	$h_1 = 3.39, h_2 = 3.40$
B	0.092	$h_1 = 3.11, h_2 = 3.12$
NR1	0.082	$h_1 = 3.10, h_2 = 3.11$
NR2	0.071	$h_1 = 3.13, h_2 = 3.14$
BR1	0.129	$h_1 = 2.52, h_2 = 2.53$
BR2	0.128	$h_1 = 2.61, h_2 = 2.62$
BR3	0.126	$h_1 = h_2 = 2.65$
BR4	0.127	$h_1 = h_2 = 2.63$
BR5	0.146	$h_1 = 2.53, h_2 = 2.55$
BR6	0.114	$h_1 = 2.68, h_2 = 2.74$
BR7	0.147	$h_1 = h_2 = 2.36$
BR8	0.141	$h_1 = 2.39, h_2 = 2.49$
BR9	0.168	$h_1 = 2.30, h_2 = 2.40$

addition, the spin density of the adsorbed O_2 molecule shown in Figure 6d–f exhibits the donut-shaped feature of the $pp\pi^*$ orbital, similar to that of a free O_2 molecule. Simultaneously, the neighboring $\text{C}_{\text{nn-O}}$ atoms display weak magnetization, with small spin moments ranging from 0.02 to $0.04 \mu_B$. Although the spin densities of O_2 and NV in Figure 6d–f seem to be uncoupled, there are significant exchange interactions between them. Intriguingly, the magnetic ground state for the $\text{O}_2\text{-NV}$ pairing fluctuates as the depth of the NV center increases, exhibiting antiferromagnetic (AFM), ferromagnetic (FM), and antiferromagnetic behavior for the N3V4, NSV6, and N8V9 cases, respectively.

We can now examine the mechanism of exchange coupling between the spins of O_2 and NV. For the N3V4 configuration, the $\text{C}_{\text{nn-V}}$ in the third layer exhibits a positive spin density, as shown in Figure 6d, while the other two $\text{C}_{\text{nn-V}}$ in the fifth layer display very weak magnetizations. The induced spin density around $\text{C}_{\text{nn-V}}$ tends to alternate in sign with every layer, whereas the spin density of $\text{C}_{\text{nn-O}}$ atoms shares the same sign as that of the third layer. Concurrently, O_2 is coupled antiferromagnetically to its carbon neighbors because its $pp\pi^*$ orbitals, which participate in adsorbate–substrate interactions, are in the minority spin channel. As a result, the

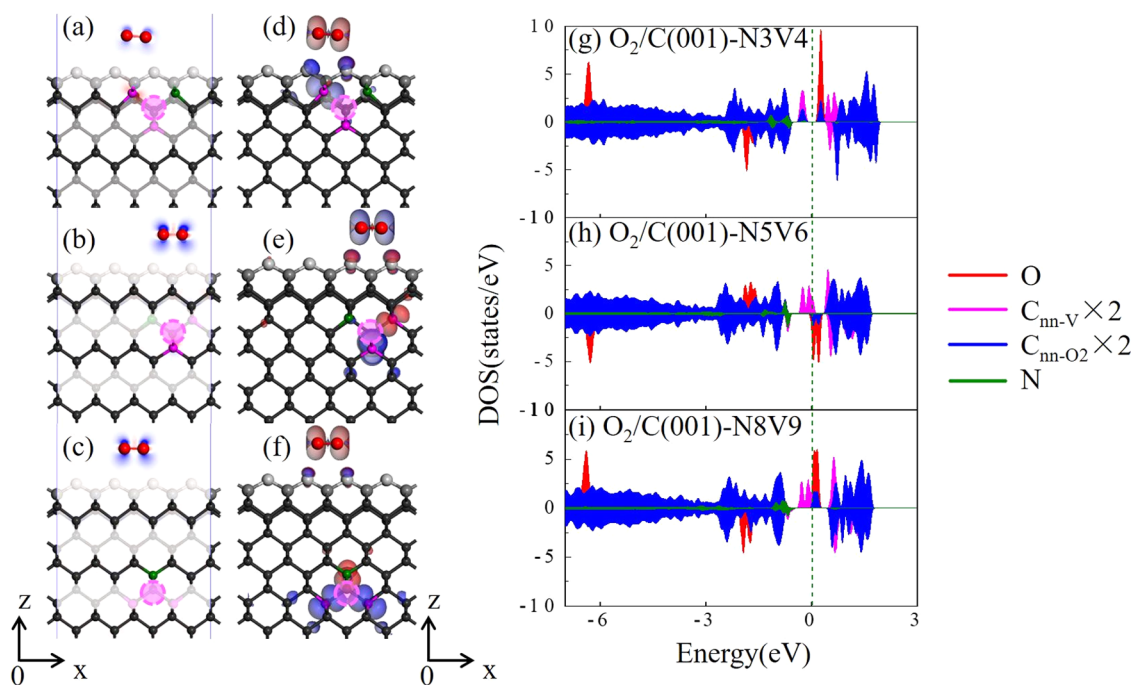


Figure 6. (a–c) Charge density differences, $\rho_{\text{O}_2/\text{C}(001)} - \rho_{\text{C}(001)} - \rho_{\text{O}_2}$, with O_2 on C(001) with the NV center at different locations. Charge accumulation and depletion are represented by blue and pink colors, respectively. (d–f) The corresponding isosurfaces of spin density ($\pm 0.001 \text{ e}/\text{\AA}^3$) are shown with blue and pink for positive and negative spin densities, respectively. Gray balls are C atoms, red balls are O atoms, green ball is N, and magenta balls are neighboring C atoms of the vacancy marked by the pink circle. (g–i) PDOS of $\text{C}_{\text{nn-v}}$ (magenta), $\text{C}_{\text{nn-O}_2}$ (blue) (both magnified by a factor of 2), O_2 (red), and N (green) atoms. The positive and negative values of PDOS correspond to states in the majority and minority spin channels, respectively.

Table 3. Magnetic Ground States (MGS), Binding Energies (E_b) (Per Adsorbate), Heights (h) of the Lowest Adatom Measured from the Topmost C Layer, Total Magnetic Moment (M), and Exchange Energies ($\Delta E_{\text{FM-AFM}}$) for O_2 , OH, and H Atom on C(001) with the NV Center at Different Depths

	GS	E_b (eV)	h (Å)	M (μ_B)	$\Delta E_{\text{FM-AFM}}$ (meV)
$\text{O}_2/\text{C}(001)\text{-N3V4}$	AFM	0.168	2.30 ($h_2 = 2.40$)	−0.997	0.3
$\text{O}_2/\text{C}(001)\text{-N5V6}$	FM	0.170	2.24 ($h_2 = 2.25$)	2.774	−0.6
$\text{O}_2/\text{C}(001)\text{-N8V9}$	AFM	0.165	2.31 ($h_2 = 2.32$)	−1.00	0.7
$\text{H}/\text{C}(001)\text{-N3V4}$	FM	3.857	1.02	2.00	−12.6
$\text{H}/\text{C}(001)\text{-N5V6}$	AFM	3.886	1.02	0	0.9
$\text{H}/\text{C}(001)\text{-N8V9}$	FM	3.890	1.02	2.00	−0.7
$\text{OH}/\text{C}(001)\text{-N3V4}$	FM	4.024	1.28	2.002	−12.7
$\text{OH}/\text{C}(001)\text{-N5V6}$	AFM	3.963	1.29	0	1.1
$\text{OH}/\text{C}(001)\text{-N8V9}$	FM	3.972	1.29	2.00	−0.6

magnetic moment of O_2 is antiparallel to that of NV in the C(001)-N3V4 configuration. In the case of N5V6, the $\text{C}_{\text{nn-v}}$ in the fifth layer possesses a negative magnetic moment, inducing a small negative spin polarization in the surface carbon layer. Consequently, the spin of the molecule of O_2 aligns with that of N5V6. The same reasoning applies to the N8V9 configuration.

In Table 3, it is noteworthy that the magnitude of the exchange energy between O_2 and NV, characterized by $\Delta E_{\text{FM-AFM}}$, is small but does not decay as rapidly as anticipated when the NV center moves away from the surface in our model calculations. This seems to be a unique feature of the C lattice in mediating the magnetic interaction, as a similar strength of the exchange coupling can also be found for H and OH with N8V9. Of course, the exchange interaction between the NV center and adsorbates is expected to decrease as the depth of NV increases further, and the magnetic dipole–dipole interaction term gradually becomes dominant. Nevertheless, it

appears that the $J(z)$ term is not negligible in the limit of depth of NV in our model. Furthermore, the torque calculations (blue lines in Figure 2d) indicate that the spin orientation of the $\text{O}_2/\text{C}(001)\text{-N3V4}$ complex remains perpendicular to the O–O bond. Consequently, the spin can almost freely rotate about the O–O bond and O_2 molecules are expected to generate significant magnetic noise at low temperatures due to the sizable exchange coupling with the NV centers.²¹

From the projected density of states of the O_2 molecule [red peaks in Figure 6g–i], it is evident that the $\text{pp}\pi^*$ orbitals of the O_2 molecule (which are in the majority spin channel for N3V4 and N8V9 but are in the minority spin channel for N5V6) shift down to the Fermi level due to the weak hybridization and charge transfer with the substrate. Some resonance can be seen due to the overlap between the PDOS curves of the O_2 and $\text{C}_{\text{nn-O}}$ atoms near the Fermi level. These states provide sufficient electron density in the carbon lattice to mediate the exchange interaction of spins, similar to the Ruderman–

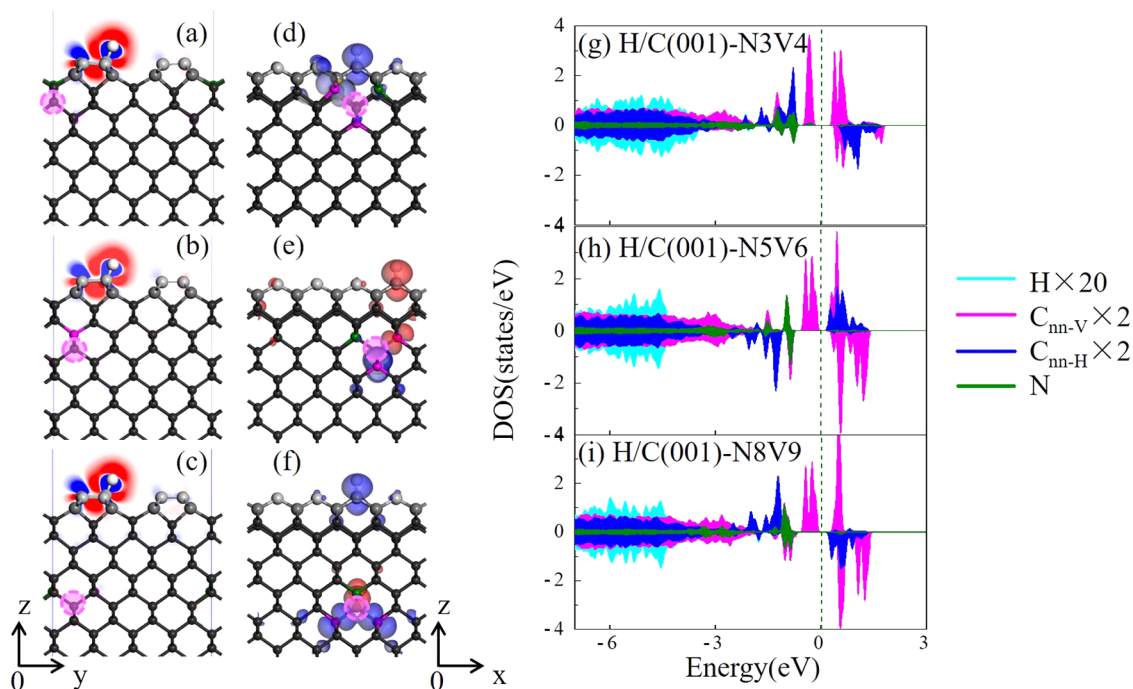


Figure 7. (a–c) Charge density differences of H adsorbed on the C(001) surface, $\rho_{\text{H/C(001)}} - \rho_{\text{C(001)}} - \rho_{\text{H}}$, with the NV center at different locations. Charge accumulation and depletion are represented by blue and red colors, respectively. (d–f) The corresponding isosurfaces of spin density ($\pm 0.001 \text{ e}/\text{\AA}^3$, blue and red for the positive and negative spin densities, respectively). Gray balls are C atoms, white ball is H, green ball is N, and magenta balls are neighboring C atoms of the vacancy marked by the pink circle. (g–i) Projected-DOS of H (cyan, magnified by a factor of 20), $C_{\text{nn-V}}$ (magenta), $C_{\text{nn-H}}$ (blue) (both magnified by a factor of 2), and N (green) atoms. The positive and negative values of PDOS correspond to states in the majority and minority spin channels, respectively.

Kittel–Kasuya–Yosida (RKKY) mechanism. As a result, we can expect a slow decay for the $J(z)$ term between O_2 and NV^- as well, although the quantitative details may vary due to the larger magnetic moment and different local spin density.

4. H and OH Adsorption on NV-Diamond Surface. In this section, we discuss the adsorption of hydrogen (H) and hydroxide (OH) on a diamond surface featuring a nitrogen-vacancy center. The interaction between these adsorbates and the NV-diamond surface can influence the properties of the surface and has implications for a variety of applications including surface chemistry, catalysis, and spintronics. It is also crucial to understand these interactions for the use of NV centers in quantum sensing and quantum information processing. Our analysis will consider factors such as the binding energy, charge transfer, and potential impact on the spin properties of the NV center.

Hydrogenated carbon surfaces are widely recognized to be more stable than clean ones under ambient conditions,^{46–48} as hydrogen coverage compensates for dangling bonds. We examined the adsorption of a single H atom at various adsorption sites, as illustrated in Figure 5b. Our DFT calculations revealed that the H atom tends to adsorb near the T2 site (Figure 5b), with large binding energies and short adsorption heights, as shown in Table 3. It is evident that the H/C(001) surface exhibits strong chemisorption with significant charge redistribution, as clearly depicted in Figure 7a–c by the charge density differences, $\rho_{\text{H/C(001)}} - \rho_{\text{C(001)}} - \rho_{\text{H}}$. Bader charge analysis indicates that H donates its 1s electron to the adjacent C atom (denoted as $C_{\text{nn-H}}$), which gains $0.09e$. The other adjacent surface carbon atoms also receive small amounts of charge, $\sim 0.02e$.

The C–H pair on the surface hosts a magnetic moment of $1.0 \mu_{\text{B}}$, with $\sim 0.42 \mu_{\text{B}}$ on the neighboring C atom. This is also clearly demonstrated by the spin density distribution in Figure 7d–f. The magnetic ground state of H/C(001) also depends on the depth of the NV; it is FM with respect to the NV center for N3V4 and N8V9 but AFM for N5V6. Interestingly, the H–NV exchange coupling is considerably stronger than that between O_2 and NV. This is due to the delocalization of the spin polarization around the H–C pair on the surface. Figure 7d demonstrates that the spin densities of N3V4 and the C–H pair are connected, leading to a direct exchange interaction between them and a large J . In the cases of N5V6 and N8V9, the exchange coupling between the spins of the C–H and NV is mediated by electrons near the Fermi level, similar to the case for the O_2 case. Consequently, the magnitude of $J(z)$ decreases to the same level as that of O_2 . As depicted in Figure 7g–i, there is no obvious hybridization between the H–C orbitals and the NV gap states near the Fermi level. The calculated MAEs of H/C(001) with and without NV are also extremely small, $\sim 0.1 \mu\text{eV}$.

The presence of hydroxyl groups on diamond surfaces, which can be derived from water vapor, has been observed in various contexts such as organic chemical reactions, wetting angle measurements, and X-ray photoelectron spectroscopy (XPS) measurements.⁴⁹ After examining all of the adsorption sites shown in Figure 5b, we found that the most stable adsorption site for OH is once again the T2 site. The binding energies listed in Table 3 are even larger than those of H, indicating the chemisorption nature of the system.

It is important to note that OH has a tilted adsorption geometry on the C(001) surface, irrespective of the depth of the NV center. The charge density differences,

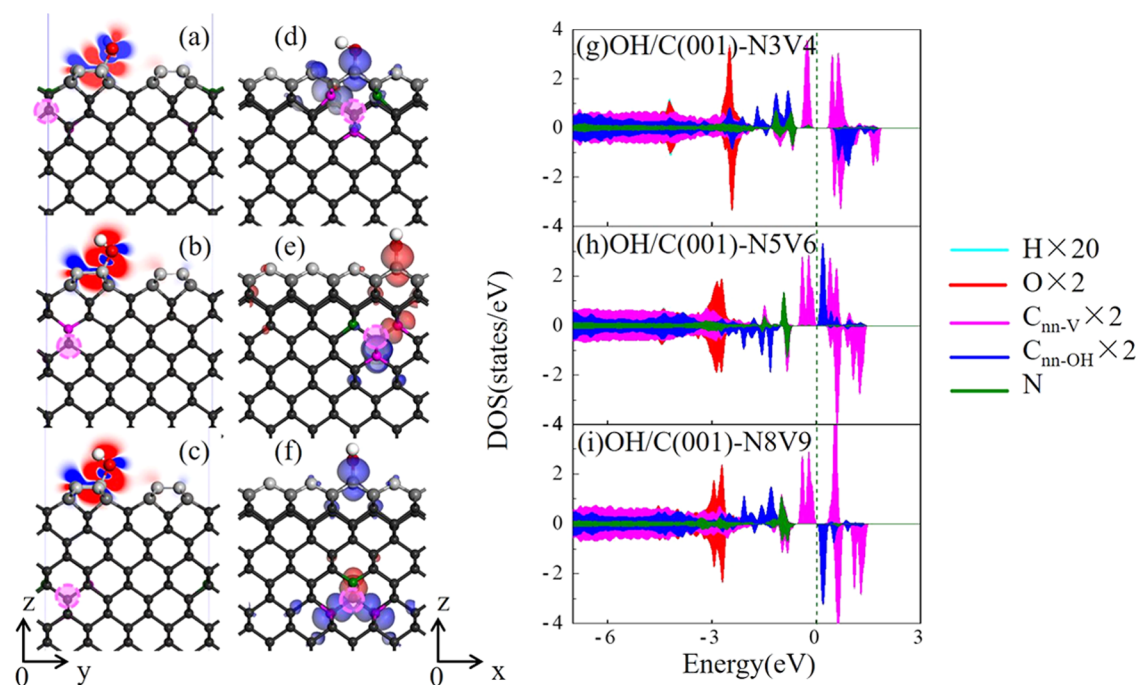


Figure 8. (a–c) Charge density differences, $\rho_{\text{OH/C}(001)} - \rho_{\text{C}(001)} - \rho_{\text{OH}}$ of OH on C(001) with the NV center at different locations. Charge accumulation and depletion are represented by blue and red colors, respectively. (d–f) The corresponding isosurfaces of spin density ($\pm 0.001 \text{ e}/\text{\AA}^3$, blue and red for the positive and negative spin densities, respectively). Gray balls are C atoms, white ball is H, red ball is O, green ball is N, and magenta balls are neighboring C atoms of the vacancy marked by the pink circle. (g–i) Projected-DOS of H (cyan, magnified by a factor of 20), O (red), $C_{\text{nn-v}}$ (magenta), $C_{\text{nn-OH}}$ (blue) (all magnified by a factor of 2), and N (green) atoms. The positive and negative values of the PDOS correspond to states in the majority and minority spin channels, respectively.

$\rho_{\text{OH/C}(001)} - \rho_{\text{C}(001)} - \rho_{\text{OH}}$, shown in Figure 8a–c, also indicate significant electron rearrangement in the surface region. These charge density differences reveal charge transfer from the nearest C atoms of the substrate to the hydroxide ions, resulting in the formation of a C–O–H group. Bader charge analysis indicates that the adsorbed O atom gets $0.88e$ and the adjacent C atom loses $1.02e$. Similar to the H adsorption case, the COH group hosts a magnetic moment of $1.0 \mu_{\text{B}}$, with approximately $0.43 \mu_{\text{B}}$ at the carbon end. The spin density distribution shown in Figure 8d–f suggests that the spin polarization is more concentrated around the oxygen atom. The PDOS curves in Figure 8g–i show no obvious adsorbate–substrate hybridization near the Fermi level. The OH orbitals are either well below or well above the Fermi level. Because of the charge transfer to OH, states of the surface carbon atom nearest OH, denoted as $C_{\text{nn-OH}}$, are shifted into the gap.

It is indeed surprising that the $J(z)$ between OH and NV is almost the same as that for the case of H in Table 2, despite the differences in their charge transfer behavior with the substrate. This indicates that the exchange coupling between spins in carbon is predominantly influenced by the subtle fluctuations in spin polarization across carbon atoms due to the magnetic defect and adsorbates. This underscores a distinctive property of carbon in mediating magnetic interactions. Given this observation, it is reasonable to expect that the exchange interaction between the NV[−] centers and various adsorbates could extend over long distances across carbon atoms. As mentioned earlier, the calculated MAEs are extremely small for OH/C(001) as well, around $0.1 \mu\text{eV}$, both with and without the presence of NV. This suggests that the magnetic fluctuations of OH can be significant and produce considerable magnetic noise.

5. Discussion. The findings in this work shed light on the sensitivity of NV probes and how they deteriorate rapidly as the NV centers approach the surface, which is attributed to the presence of adsorbates on the carbon slabs. While the dimerized C(001) surface was used as the model system in this study, it is conceivable that the adsorbates, such as O₂, H, and OH, could interact with other diamond surfaces and exhibit qualitatively similar behaviors. This means that the findings related to magnetic noise and exchange interactions may be applicable to a broader range of diamond surfaces. Additionally, the slow decay of $J(z)$ should be independent of the surface orientation. As we previously estimated based on dipole interactions, a minimum depth of 3 nm is necessary to prevent the influence of magnetic dopants on the NV center. Recent observations have supported this estimation, indicating that an optimal depth for the NV ensemble is approximately 5 nm.⁵⁰ Clearly, the presence of magnetic adsorbates needs to be carefully considered and addressed in any diamond-based NV center applications to ensure optimal performance and accuracy.

It is important to note that O₂ exhibits a low binding energy on C(001) and possibly other carbon surfaces as well. As a result, O₂ typically desorbs at relatively high temperatures, which may limit its impact, unless the NV probe operates at extremely low temperatures. Besides, O₂ can be removed from diamond surfaces using either a protective coating or ultraviolet light illumination, as mentioned for reducing 1/f magnetic noise on SQUID surfaces in refs 21,24. On the other hand, H and OH exhibit chemisorption, making them more difficult to remove. Since they are water vapor derivatives, preventing water adsorption and dissociation on the diamond surface appears to be more critical. Various approaches, such as

surface passivation using thin silicon dioxide (SiO_2) layers or hydrophobic polymer coatings, can be employed. The selection of protective materials depends on the adsorbate species and surface conditions. Further research in this area will undoubtedly be valuable in identifying effective strategies for NV probes.

While directly simulating NV^- for NV probe development is preferable, achieving electronic and structural convergence for many configurations with adsorbates on carbon slabs with charged NV^- centers proved challenging, even with recent methods like the self-consistent potential correction approach.²⁶ Furthermore, NV^- has a multiconfigurational ground state which cannot be described accurately in ordinary DFT. This prevented us from making direct comparisons with rich experimental data established in the literature. However, the slow decline of both exchange coupling and magnetic dipole interaction is expected to be independent of the charge state of the NV center. This implies that surface noise poses a critical concern for both NV^0 and NV^- states, providing that magnetic adsorbates are in proximity.

Additionally, the electronic properties of NV centers can be significantly affected by the presence of adsorbates beyond the magnetic interactions. Hauf et al. have shown that changes in surface termination can lead to the conversion of stable NV^- centers into NV^0 and an unknown nonfluorescent state, due to band bending.⁵¹ The present studies also indicated that the gap states exhibit noticeable changes due to the presence of O_2 , H, and OH, as evidenced by the DOS curves shown in Figures 6–8, even in the case of N8V9 . As the changes of electronic states are at the meV level and the energy splitting between spin states (e.g., $S_z = +1/2$ and $-1/2$ for NV^0) due to the exchange coupling can be up to 100 GHz (a few tenths of meV) for the deepest NV center in our model, we perceive that the ODMR measurement is essentially impossible.

Finally, Kim et al. have reported that electric-field noise can be more impactful than magnetic field noise for NV probe and they found that adding a protective surface layer such as deuterated glycerol can reduce electric-field noise.⁵² Multiple approaches, including varying surface patterning, cleaning methods, and coating layers, have been explored and tested.^{53,54} Janitz et al. provided a comprehensive review of potential sources of charge-state instability and decoherence for near-surface NV centers, including band bending, charge trapping, surface roughness, surface spin, and unscreened charge.⁵⁵ Our research has identified specific adsorbates that contribute to these effects and may aid in targeted magnetic noise reduction efforts.

IV. CONCLUSIONS

In summary, our systematic DFT calculations have demonstrated that the adsorption of O_2 on the C(001) surface can be stably adsorbent at low temperatures and retain a sizable magnetic moment of $2.0 \mu_B$. Additionally, H and OH also exhibit magnetic moments of $1.0 \mu_B$ on diamond, even though they have strong chemical interactions with the surface. These moments may significantly disturb the quantum spin states of the NV center through either magnetic dipole interaction in a range of up to 3 nm or through non-negligible exchange interactions, even when the NV center is 8 layers below the surface. This slow decay implies that even at greater distances, the magnetic adsorbates can still significantly influence the NV center's behavior regardless of the NV center's charge state. The magnetic anisotropy barrier energies of adsorbates like O_2 ,

H, and OH are exceedingly small (smaller than $1 \mu\text{eV}$ per molecule or atom). Due to these low energies, the adsorbates' magnetic moments can easily fluctuate in response to even minor changes in their environment, which may interfere with the performance of NV centers in quantum sensing and other applications. Our research emphasizes the need to consider various potential magnetic sources that might adversely affect NV probes and highlights the significance of removing surface adsorbates in this regard.

AUTHOR INFORMATION

Corresponding Author

R. Q. Wu – Department of Physics and Astronomy, University of California, Irvine, California 92697-4575, United States; orcid.org/0000-0002-6156-7874; Email: wur@uci.edu

Authors

P. J. Zuo – State Key Laboratory of Surface Physics, Key Laboratory of Computational Physical Sciences, and Department of Physics, Fudan University, Shanghai 200433, China

Z. Wang – State Key Laboratory of Surface Physics, Key Laboratory of Computational Physical Sciences, and Department of Physics, Fudan University, Shanghai 200433, China

Clare C. Yu – Department of Physics and Astronomy, University of California, Irvine, California 92697-4575, United States

Complete contact information is available at: <https://pubs.acs.org/10.1021/acs.jpcc.3c04026>

Notes

The authors declare no competing financial interest.

ACKNOWLEDGMENTS

The research presented was supported by the U.S. Department of Energy's Office of Science, Basic Energy Sciences, under Award DE-FG02-05ER46237 and a computational resource provided by the National Energy Research Scientific Computing Center. C.C.Y. extends gratitude to Prof. Amir Yacoby for insightful discussions during a visit to the Aspen Center for Physics, which is backed by the National Science Foundation under Grant PHY-1607611.

REFERENCES

- (1) Rondin, L.; Tetienne, J. P.; Hingant, T.; Roch, J. F.; Maletinsky, P.; Jacques, V. Magnetometry with nitrogen-vacancy defects in diamond. *Rep. Prog. Phys.* **2014**, *77*, 056503.
- (2) Hong, S.; Grinolds, M. S.; Pham, L. M.; Le Sage, D.; Luan, L.; Walsworth, R. L.; Yacoby, A. Nanoscale magnetometry with NV centers in diamond. *MRS Bull.* **2013**, *38*, 155.
- (3) Schirhagl, R.; Chang, K.; Loretz, M.; Degen, C. L. Nitrogen-Vacancy Centers in Diamond: Nanoscale Sensors for Physics and Biology. *Annu. Rev. Phys. Chem.* **2014**, *65*, 83.
- (4) Casola, F.; van der Sar, T.; Yacoby, A. Probing condensed matter physics with magnetometry based on nitrogen-vacancy centres in diamond. *Nat. Rev. Mater.* **2018**, *3* (1), No. 17088.
- (5) Childress, L.; Hanson, R. Diamond NV centers for quantum computing and quantum networks. *MRS Bull.* **2013**, *38*, 134.
- (6) Chernobrod, B. M.; Berman, G. P. Spin microscope based on optically detected magnetic resonance. *J. Appl. Phys.* **2005**, *97*, 014903.
- (7) Balasubramanian, G.; Chan, I. Y.; Kolesov, R.; Al-Hmoud, M.; Tisler, J.; Shin, C.; Kim, C.; Wojcik, A.; Hemmer, P. R.; Krueger, A.;

- et al. Nanoscale imaging magnetometry with diamond spins under ambient conditions. *Nature* **2008**, *455*, 648.
- (8) Degen, C. L. Scanning magnetic field microscope with a diamond single-spin sensor. *Appl. Phys. Lett.* **2008**, *92*, 243111.
- (9) Fu, C.-C.; Lee, H.-Y.; Chen, K.; Lim, T.-S.; Wu, H.-Y.; Lin, P.-K.; Wei, P.-K.; Tsao, P.-H.; Chang, H.-C.; Fann, W. Characterization and application of single fluorescent nanodiamonds as cellular biomarkers. *Proc. Natl. Acad. Sci. U.S.A.* **2007**, *104*, 727.
- (10) Roskopf, T.; Dussaux, A.; Ohashi, K.; Loretz, M.; Schirhagl, R.; Watanabe, H.; Shikata, S.; Itoh, K. M.; Degen, C. L. Investigation of Surface Magnetic Noise by Shallow Spins in Diamond. *Phys. Rev. Lett.* **2014**, *112*, 147602.
- (11) Hensen, B.; Bernien, H.; Dréau, A. E.; Reiserer, A.; Kalb, N.; Blok, M. S.; Ruitenberg, J.; Vermeulen, R. F. L.; Schouten, R. N.; Abellán, C.; et al. Loophole-free Bell inequality violation using electron spins separated by 1.3 kilometres. *Nature* **2015**, *526*, 682.
- (12) Gali, A. Ab initio theory of the nitrogen-vacancy center in diamond. *Nanophotonics* **2019**, *8*, 1907.
- (13) Degen, C. L.; Reinhard, F.; Cappellaro, P. Quantum sensing. *Rev. Mod. Phys.* **2017**, *89*, 035002.
- (14) Doherty, M. W.; Manson, N. B.; Delaney, P.; Jelezko, F.; Wrachtrup, J.; Hollenberg, L. C. L. The nitrogen-vacancy colour centre in diamond. *Phys. Rep.* **2013**, *528*, 1.
- (15) Loretz, M.; Pezzagna, S.; Meijer, J.; Degen, C. L. Nanoscale nuclear magnetic resonance with a 1.9-nm-deep nitrogen-vacancy sensor. *Appl. Phys. Lett.* **2014**, *104*, 033102.
- (16) Oliveira, F. F. d.; Momenzadeh, S. A.; Wang, Y.; Konuma, M.; Markham, M.; Edmonds, A. M.; Denisenko, A.; Wrachtrup, J. Effect of Low-Damage Inductively Coupled Plasma on Shallow Nitrogen-Vacancy Centers in Diamond. *Appl. Phys. Lett.* **2015**, *107* (7), 073107 DOI: 10.1063/1.4929356.
- (17) Li, S.; Chou, J.-P.; Wei, J.; Sun, M.; Hu, A.; Gali, A. Oxygenated (113) diamond surface for nitrogen-vacancy quantum sensors with preferential alignment and long coherence time from first principles. *Carbon* **2019**, *145*, 273.
- (18) Wang, J.; Zhang, W.; Zhang, J.; You, J.; Li, Y.; Guo, G.; Feng, F.; Song, X.; Lou, L.; Zhu, W.; Wang, G. Coherence times of precise depth controlled NV centers in diamond. *Nanoscale* **2016**, *8*, 5780.
- (19) Chrostoski, P.; Barrios, B.; Santamore, D. H. Magnetic field noise analyses generated by the interactions between a nitrogen vacancy center diamond and surface and bulk impurities. *Phys. B* **2021**, *605*, 412767.
- (20) Jiang, Y.; Zhang, Y. N.; Cao, J. X.; Wu, R. Q.; Ho, W. Real-Space Imaging of Kondo Screening in a Two-Dimensional O₂ Lattice. *Science* **2011**, *333*, 324.
- (21) Wang, H.; Shi, C. T.; Hu, J.; Han, S. H.; Yu, C. C.; Wu, R. Q. Candidate Source of Flux Noise in SQUIDS: Adsorbed Oxygen Molecules. *Phys. Rev. Lett.* **2015**, *115* (5), 077002.
- (22) Kumar, P.; Sendelbach, S.; Beck, M. A.; Freeland, J. W.; Wang, Z.; Wang, H.; Yu, C. C.; Wu, R. Q.; Pappas, D. P.; McDermott, R. Origin and Reduction of 1/f Magnetic Flux Noise in Superconducting Devices. *Phys. Rev. Appl.* **2016**, *6*, 041001.
- (23) de Graaf, S. E.; Adamy, A. A.; Lindström, T.; Erts, D.; Kubatkin, S. E.; Tzalenchuk, A. Y.; Danilov, A. V. Direct Identification of Dilute Surface Spins on Al₂O₃: Origin of Flux Noise in Quantum Circuits. *Phys. Rev. Lett.* **2017**, *118*, 057703.
- (24) Wang, Z.; Wang, H.; Yu, C. C.; Wu, R. Q. Hydrogen as a source of flux noise in SQUIDS. *Phys. Rev. B* **2018**, *98* (5), 020403.
- (25) Löfgren, R.; Pawar, R.; Öberg, S.; Larsson, J. A. The bulk conversion depth of the NV-center in diamond: computing a charged defect in a neutral slab. *New J. Phys.* **2019**, *21*, 053037.
- (26) Chagas da Silva, M.; Lorke, M.; Aradi, B.; Tabriz, M. F.; Frauenheim, T.; Rubio, A.; Rocca, D.; Deák, P. Self-Consistent Potential Correction for Charged Periodic Systems. *Phys. Rev. Lett.* **2021**, *126*, 076401.
- (27) Singh, J. *Physics of Semiconductors and their Heterostructures*; McGraw-Hill College, 1993.
- (28) Kresse, G.; Hafner, J. Ab initio molecular-dynamics simulation of the liquid-metal–amorphous-semiconductor transition in germanium. *Phys. Rev. B* **1994**, *49*, 14251–14269.
- (29) Kresse, G.; Furthmüller, J. Efficient iterative schemes for ab initio total-energy calculations using a plane-wave basis set. *Phys. Rev. B* **1996**, *54*, 11169.
- (30) Perdew, J. P.; Burke, K.; Ernzerhof, M. Generalized Gradient Approximation Made Simple. *Phys. Rev. Lett.* **1996**, *77*, 3865.
- (31) Kresse, G.; Joubert, D. From ultrasoft pseudopotentials to the projector augmented-wave method. *Phys. Rev. B* **1999**, *59*, 1758.
- (32) Blöchl, P. E. Projector augmented-wave method. *Phys. Rev. B* **1994**, *50*, 17953.
- (33) Monkhorst, H. J.; Pack, J. D. Special points for Brillouin-zone integrations. *Phys. Rev. B* **1976**, *13*, 5188.
- (34) Wu, R. Q.; Freeman, A. J. Spin-orbit induced magnetic phenomena in bulk metals and their surfaces and interfaces. *J. Magn. Magn. Mater.* **1999**, *200*, 498.
- (35) Hu, J.; Wu, R. Control of the Magnetism and Magnetic Anisotropy of a Single-Molecule Magnet with an Electric Field. *Phys. Rev. Lett.* **2013**, *110*, 097202.
- (36) Pate, B. B. The diamond surface: atomic and electronic structure. *Surf. Sci.* **1986**, *165*, 83.
- (37) Hamza, A. V.; Kubiak, G. D.; Stulen, R. H. Hydrogen chemisorption and the structure of the diamond C(100)-(2 × 1) surface. *Surf. Sci.* **1990**, *237*, 35.
- (38) Goss, J. P.; Briddon, P. R.; Papagiannidis, S.; Jones, R. Interstitial nitrogen and its complexes in diamond. *Phys. Rev. B* **2004**, *70*, 235208.
- (39) Goss, J. P.; Briddon, P. R.; Rayson, M. J.; Sque, S. J.; Jones, R. Vacancy-impurity complexes and limitations for implantation doping of diamond. *Phys. Rev. B* **2005**, *72*, 035214.
- (40) Furthmüller, J.; Hafner, J.; Kresse, G. Dimer reconstruction and electronic surface states on clean and hydrogenated diamond (100) surfaces. *Phys. Rev. B* **1996**, *53*, 7334.
- (41) Sque, S. J.; Jones, R.; Briddon, P. R. Structure, electronics, and interaction of hydrogen and oxygen on diamond surfaces. *Phys. Rev. B* **2006**, *73*, 085313.
- (42) Mackey, B. L.; Russell, J. N.; Crowell, J. E.; Pehrsson, P. E.; Thoms, B. D.; Butler, J. E. Oxygen Adsorption on the (110)-Oriented Diamond Surface. *J. Phys. Chem. B* **2001**, *105*, 3803.
- (43) Bobrov, K.; Shechter, H.; Hoffman, A.; Folman, M. Molecular oxygen adsorption and desorption from single crystal diamond (1 1 1) and (1 1 0) surfaces. *Appl. Surf. Sci.* **2002**, *196*, 173.
- (44) Wang, X.; Wu, R.; Wang, D.-s.; Freeman, A. Torque method for the theoretical determination of magnetocrystalline anisotropy. *Phys. Rev. B* **1996**, *54*, 61.
- (45) Gali, A. Theory of the neutral nitrogen-vacancy center in diamond and its application to the realization of a qubit. *Phys. Rev. B* **2009**, *79*, 235210.
- (46) Krueger, A.; Lang, D. Functionality is Key: Recent Progress in the Surface Modification of Nanodiamond. *Adv. Funct. Mater.* **2012**, *22*, 890.
- (47) Krüger, A.; Liang, Y.; Jarre, G.; Stegk, J. Surface functionalisation of detonation diamond suitable for biological applications. *J. Mater. Chem.* **2006**, *16*, 2322.
- (48) Shenderova, O.; Panich, A. M.; Moseenkova, S.; Hens, S. C.; Kuznetsov, V.; Vieth, H. M. Hydroxylated detonation nanodiamond: FTIR, XPS, and NMR studies. *J. Phys. Chem. C* **2011**, *115* (39), 19005–19011.
- (49) Boukherroub, R.; Wallart, X.; Szunerits, S.; Marcus, B.; Bouvier, P.; Mermoux, M. Photochemical oxidation of hydrogenated boron-doped diamond surfaces. *Electrochem. Commun.* **2005**, *7*, 937.
- (50) Henshaw, J.; Kehayias, P.; Ziabari, M. S.; Titze, M.; Morissette, E.; Watanabe, K.; Taniguchi, T.; Li, J. I. A.; Acosta, V. M.; Bielejec, E. S.; et al. Nanoscale solid-state nuclear quadrupole resonance spectroscopy using depth-optimized nitrogen-vacancy ensembles in diamond. *Appl. Phys. Lett.* **2022**, *120*, 174002.
- (51) Hauf, M. V.; Grotz, B.; Naydenov, B.; Dankerl, M.; Pezzagna, S.; Meijer, J.; Jelezko, F.; Wrachtrup, J.; Stutzmann, M.; Reinhard, F.;

Garrido, J. A. Chemical control of the charge state of nitrogen-vacancy centers in diamond. *Phys. Rev. B* **2011**, *83* (8), 081304.

(52) Kim, M.; Mamin, H. J.; Sherwood, M. H.; Ohno, K.; Awschalom, D. D.; Rugar, D. Decoherence of Near-Surface Nitrogen-Vacancy Centers Due to Electric Field Noise. *Phys. Rev. Lett.* **2015**, *115*, 087602.

(53) Mamin, H. J.; Kim, M.; Sherwood, M. H.; Rettner, C. T.; Ohno, K.; Awschalom, D. D.; Rugar, D. Nanoscale Nuclear Magnetic Resonance with a Nitrogen-Vacancy Spin Sensor. *Science* **2013**, *339*, 557.

(54) Chrostoski, P.; Sadeghpour, H. R.; Santamore, D. H. Electric Noise Spectra of a Near-Surface Nitrogen-Vacancy Center in Diamond with a Protective Layer. *Phys. Rev. Appl.* **2018**, *10*, 064056.

(55) Janitz, E.; Herb, K.; Völker, L. A.; Huxter, W. S.; Degen, C. L.; Abendroth, J. M. Diamond surface engineering for molecular sensing with nitrogen—vacancy centers. *J. Mater. Chem. C* **2022**, *10*, 13533–13569.